Editors' Suggestion | Featured in Physics

# Observation of Exceptional Points in Thermal Atomic Ensembles

Chao Liang,[1] Yuanjiang Tang,[1] An-Ning Xu,[1] and Yong-Chun Liu[1,2,*]
[1]State Key Laboratory of Low-Dimensional Quantum Physics, Department of Physics, Tsinghua University, Beijing 100084, China
[2]Frontier Science Center for Quantum Information, Beijing 100084, China

(Received 1 December 2022; accepted 13 April 2023; published 28 June 2023)

Exceptional points (EPs) in non-Hermitian systems have recently attracted wide interest and spawned intriguing prospects for enhanced sensing. However, EPs have not yet been realized in thermal atomic ensembles, which is one of the most important platforms for quantum sensing. Here we experimentally observe EPs in multilevel thermal atomic ensembles and realize enhanced sensing of the magnetic field for 1 order of magnitude. We take advantage of the rich energy levels of atoms and construct effective decays for selected energy levels by employing laser coupling with the excited state, yielding unbalanced decay rates for different energy levels, which finally results in the existence of EPs. Furthermore, we propose the optical polarization rotation measurement scheme to detect the splitting of the resonance peaks, which makes use of both the absorption and dispersion properties and shows an advantage with enhanced splitting compared with the conventional transmission measurement scheme. Additionally, in our system both the effective coupling strength and decay rates are flexibly adjustable, and thus the position of the EPs are tunable, which expands the measurement range. Our Letter not only provides a new controllable platform for studying EPs and non-Hermitian physics, but also provide new ideas for the design of EP-enhanced sensors and opens up realistic opportunities for practical applications in the high-precision sensing of magnetic field and other physical quantities.

DOI: 10.1103/PhysRevLett.130.263601

Non-Hermitian physics has been one of the research highlights in recent years [1,2]. Compared with the Hermitian Hamiltonians, non-Hermitian Hamiltonians have many interesting and unique properties, where one of the prominent examples is non-Hermitian degeneracies, also known as exceptional points (EPs) [3–5]. An EP occurs when two or more eigenvalues and the corresponding eigenstates coalesce, simultaneously, which is impossible for Hermitian Hamiltonians. In the vicinity of EPs, complex energies of a non-Hermitian system can lead to novel phenomenon that cannot appear in their Hermitian counterparts. For example, when two degenerate eigenmodes are lifted by a perturbation $\epsilon$, the eigenfrequency splitting $\Delta\omega$ satisfies a square-root law, i.e., $\Delta\omega \propto \sqrt{\epsilon}$, which is very different from Hermitian cases where signals scale linearly with the perturbation $\epsilon$ [6–9]. Obviously, this sublinear response signifies an enhanced measurement sensitivity $\propto 1/\sqrt{\epsilon}$ in the small perturbation limit $\epsilon \to 0$, which can be used to design EP-enhanced sensors. In recent years, EPs have been studied in many systems, e.g., optical microcavities [10–19], photonic crystal slabs [20,21], and acoustic [22], circuit [23–28], optomechanical [29,30], and superconducting systems [31–33], as well as ultracold atoms [34], trapped ions [35], atomic systems [36–41], and nitrogen-vacancy centers [42].

However, EPs have not yet been realized in thermal atomic ensembles, which is one of the most important platforms for exploring quantum precision measurement and quantum sensors, e.g., ultrasensitive magnetometers [43–45], gyroscopes [46], electrometers [47,48] and atomic clocks [49]. Therefore, it is urgent to achieve EPs and design EP-enhanced sensing schemes in thermal atomic ensembles, so that we can take advantage of the non-Hermitian features for practical applications in a vast variety of sensors.

Here we propose a new paradigm for studying the non-Hermitian physics by taking advantage of the rich energy level structure and couplings in thermal atomic ensembles. We experimentally observe EPs in thermal atomic ensembles and realize enhanced sensing of the magnetic field, for the first time as far as we know. Moreover, instead of measuring the transmission spectrum in conventional studies, we propose a new protocol relying on the optical polarization rotation signal to detect the resonance peak splitting, which can enhance the frequency splitting and is robust to the noises. We demonstrate that peak splitting of the optical rotation signal scales as the square root of the

perturbation magnetic field strength and maintain a high sensitivity for weak perturbation. In addition, in our system, most experimental parameters are flexibly adjustable, so we can move the position of the EP to expand the measurement range of the magnetic field. Therefore, this Letter opens up realistic opportunities for practical applications in high-precision sensing of the magnetic field.

Our model is based on a four-level atomic system as shown in Fig. 1(a). There are three Zeeman sublevels of ground state $|0\rangle$, $|1\rangle$, and $|2\rangle$, which are coupled by an oscillating radio-frequency (rf) magnetic field. A laser drives the transition from the ground state $|1\rangle$ to the excited state $|3\rangle$. Their Rabi frequencies and the detunings of coupling fields above from their coupled transitions are denoted by $(J_0, J_0, \Omega_0)$ and $(\delta, \delta, \Delta)$, respectively. The spontaneous decay rate of the excited state $|3\rangle$ is $\Gamma$ and the relaxation rate of the Zeeman sublevels is $\gamma_0$, which

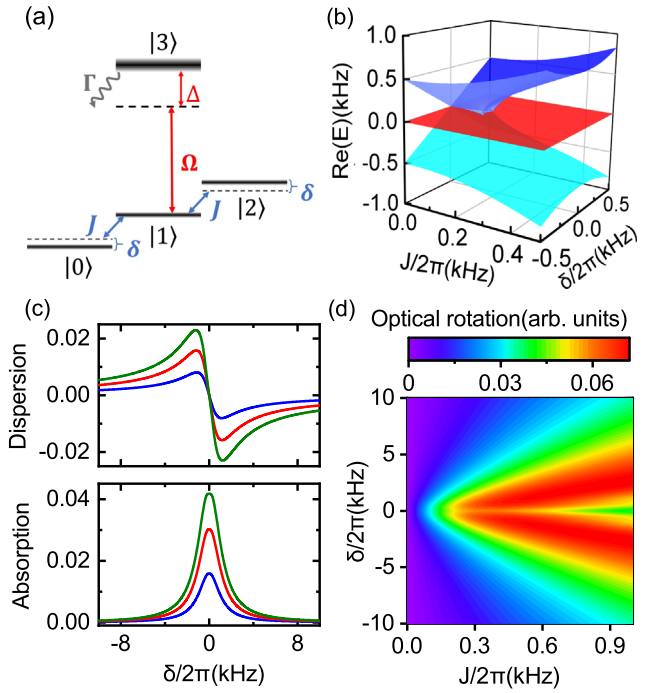


FIG. 1. System model for observing EPs in atomic ensembles. (a) Atomic energy level diagrams. $\Gamma$ denotes the spontaneous decay rate of the excited state $|3\rangle$. $J$ denotes the effective coupling rate from an applied oscillating rf magnetic field with frequency detuning $\delta$ relative to the transition of adjacent Zeeman levels $|0\rangle$, $|1\rangle$, $|2\rangle$. The probe lasers drive the transition $|1\rangle \Leftrightarrow |3\rangle$ with the detuning $\Delta$ and the effective Rabi frequency is $\Omega$. (b) The real parts of the eigenvalues of $H_{\mathrm{NH}}$ in Eq. (2) as a function of $\delta$ and $J$. (c) The absorption $S_{\mathrm{abs}}$ and dispersion $S_{\mathrm{disp}}$ curves of the optical polarization rotation signal for different rf Rabi frequency $J/2\pi$ being 0.05 (blue curve), 0.10 (red curve), and 0.15 kHz (green curve), respectively. (d) Color map of the magnitude of the optical polarization rotation signal versus detuning $\delta$ for various values of $J$. Other parameters are specified in the main text.

satisfies $\gamma_0 \ll \Gamma$. In the rotating reference frame, the Hamiltonian reads [50]

$$H = \begin{pmatrix} -\delta & J & 0 & 0 \\ J & 0 & J & -\Omega \\ 0 & J & \delta & 0 \\ 0 & -\Omega & 0 & -\Delta \end{pmatrix}, \tag{1}$$

where $J = J_0/(2\sqrt{2})$ is the effective rf Rabi frequencies and $\Omega = \Omega_0/(2\sqrt{3})$ is the effective optical Rabi frequencies. The evolution of the density matrix $\rho$ is described by the master equation $\dot{\rho} = -i[H, \rho] + \mathcal{L}[\rho]$, where $\mathcal{L}$ is the Lindblad operator describing the decay and dephasing of the system. When the decay rate $\Gamma$ is much greater than all other rates, we can eliminate the excited state $|3\rangle$ and obtain the effective non-Hermitian Hamiltonian $H_{\mathrm{NH}}$ governing the dynamics of the ground sublevels [50] (set $\Delta = 0$ for simplicity),

$$H_{\mathrm{NH}} = \begin{pmatrix} -\delta & J & 0 \\ J & -\frac{i}{2}\gamma_{\mathrm{opt}} & J \\ 0 & J & \delta \end{pmatrix}. \tag{2}$$

Here $\gamma_{\mathrm{opt}} = 4\ \Omega^2/\Gamma$ corresponds to an effective decay rate for state $|1\rangle$, which is the key factor to realize the effective non-Hermitian Hamiltonian. This effective decay rate $\gamma_{\mathrm{opt}}$ originates from the laser-driven coupling between state $|1\rangle$ and state $|3\rangle$, where the strong decay of state $|3\rangle$ results in the effective decay of state $|1\rangle$. Similar effective non-Hermitian Hamiltonians have been studied in the anti-parity-time-symmetry system [51–53].

When $\delta = 0$, the three eigenvalues of $H_{\mathrm{NH}}$ are given by

$$E_0 = 0, \qquad E_{\pm} = -i\kappa\gamma_0 \pm \sqrt{2J^2 - \kappa^2\gamma_0^2}, \tag{3}$$

where $\kappa = \Omega^2/(\Gamma\gamma_0)$ is the dimensionless saturation parameter of the probe laser. As shown in Eq. (3), in the case of $J = J_{\mathrm{EP}} \equiv \kappa\gamma_0/\sqrt{2}$, the real [Fig. 1(b)] and imaginary parts of the eigenvalues $E_{\pm}$ will degenerate simultaneously, corresponding to the EPs. Thus, the system possesses second-order EPs and it behaves like a $\mathcal{PT}$-symmetry two-level system [54]. When $J < J_{\mathrm{EP}}$, the complex eigenvalues have different imaginary parts, and the system is in the $\mathcal{PT}$-symmetry-broken-like phase. On crossing the EP with $J > J_{\mathrm{EP}}$, the imaginary parts of the eigenvalues $E_{\pm}$ coincide, and the system is in the $\mathcal{PT}$-symmetrylike phase.

In the parametric space consisting of the effective rf Rabi frequencies $J$ and the saturation parameters $\kappa$, the EPs are joined to form exceptional arcs that satisfy $J = \kappa\gamma_0/\sqrt{2}$. Remarkably, in our system, the parameters $J$ and $\kappa$ can be freely tuned by adjusting the rf and optical driving strength, which correspond to the magnetic filed strength and laser power, respectively. Thus, it enables free control of the

position of EPs and is promising for designing EP-enhanced sensors with broad measurement range.

Furthermore, third-order EPs can also be obtained as long as the sublevels of ground state $|0\rangle$, $|1\rangle$, and $|2\rangle$ have different effective decay rates, which can be realized by using similar laser-driven couplings $|0\rangle \Leftrightarrow |3\rangle$ and $|2\rangle \Leftrightarrow |3\rangle$ [50]. This provides more possibilities for studying high-order non-Hermitian physics with thermal atomic systems.

The system eigenstates can be experimentally probed by slowly sweeping the detuning $\delta$ of the rf magnetic field with time and measuring the optical polarization rotation (OPR) signal of the probe laser. The magnitude of the OPR signal is composed of an absorptive part and a dispersive part. The expectation value of the absorptive ($S_{\rm abs}$) and dispersive signal ($S_{\rm dis}$) is found from the density matrix of ground states [50],

$$S_{\rm abs} \propto {\rm Re}(\rho_{10} - \rho_{21}), \qquad S_{\rm dis} \propto {\rm Im}(\rho_{10} - \rho_{21}), \quad (4)$$

where density matrix elements $\rho_{10}$ and $\rho_{21}$ represent the coherences between Zeeman sublevels. Typical absorption and dispersion profiles versus $\delta$ are shown in Fig. 1(c). We can further define the magnitude of the OPR signal as $S = \sqrt{S_{\rm abs}^2 + S_{\rm dis}^2}$. The color map of optical polarization rotation magnitude versus $J$ and $\delta$ is plotted in Fig. 1(d). It shows that as $J$ increases, the resonance peak splits into two peaks, and the positions of the peaks can be derived as [50]

$$f_{\pm}(J) = \begin{cases} 0 & \text{if } J < J_{\rm OPR}, \\ \pm\sqrt{2J_{\rm OPR}(J - J_{\rm OPR})} & \text{if } J \geq J_{\rm OPR}, \end{cases} \quad (5)$$

where $J_{\rm OPR}$ is the peak splitting parameter of the OPR signal with the expression $J_{\rm OPR} = \gamma_0\sqrt{(8\kappa^2 + 6\kappa + 1)/\{8\kappa[16\kappa(2\kappa + 3) + 21] + 26\}}$. It reveals that the peak positions $f_{\pm}(J)$ have square-root response when $J \geq J_{\rm OPR}$, and such a sublinear response provides the opportunity for EP-enhanced sensing.

Based on the above theoretical model, we design the experiment with the schematic diagram shown in Fig. 2. A cubic paraffin-coated glass cell (side length 1 cm), surrounded by a two-layer $\mu$-metal magnetic shield, is filled with $^{87}$Rb atoms. The temperature of the cell is stabilized at 50 °C. The combination of one pair of Helmholtz coils and two pairs of gradient and uniform saddle coils [55], which is placed inside the innermost shield, is used to compensate the residual magnetic fields and to create static ($B_z = B_0$ in the $z$ direction) and oscillating fields [$B_x = B_{\rm rf}\cos(\omega t)$ in the $x$ direction]. The typical static field strength $B_0$ is 0.65 G, which gives a ground-state Zeeman splitting of $\Omega_L/2\pi = 453$ kHz. A $z$-polarized probe laser propagating through the vapor cell along the $x$ axis is red detuned by 700 MHz from the $|5^2S_{1/2}, F = 2, m_F = 0\rangle \Leftrightarrow |5^2P_{1/2}, F = 1, m_F = 0\rangle (|1\rangle \Leftrightarrow |3\rangle)$ transition of the D1 line. The light intensity is 5 μW unless otherwise specified and the beam diameter is ∼4 mm. After passing through the vapor cell, the polarization of the laser is analyzed using a balanced polarimeter setup and extracted by the lock-in amplifier.

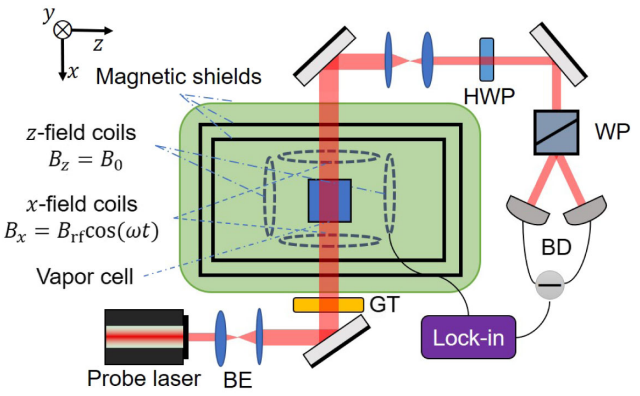


FIG. 2. Schematic diagram of the experimental setup. A laser beam linearly polarized along the $z$ axis propagates through a paraffin-coated vapor cell that is filled with rubidium-87 ($^{87}$Rb) atoms. A constant $z$-direction magnetic field $B_0$ and an oscillating $x$-direction rf magnetic field $B_x = B_{\rm rf}\cos(\omega t)$ are applied within the magnetic shields that surround the cell. The lock-in amplifier is used to analyze the OPR signal. BE, beam expansion module; GT, Glan-Taylor polarizer; HWP, half wave plate; WP, Wollaston prism; BD, balanced detection.

The EPs are observed experimentally using the above setup. In Fig. 3(a), we display the measured OPR signal versus detuning $\delta$ at different rf magnetic field strengths $B_{\rm rf}$. As we fix the probe laser power $P$ and increase the strength of the rf magnetic field $B_{\rm rf}$, the resonance peak begins to split into two peaks, which means that we have swept over the EP. On the other hand, as shown in Fig. 3(b), the separation distance of the two splitting peaks will gradually decrease to disappear as we fix the $B_{\rm rf}$ and increase the probe laser power $P$. To determine the location of the EP, we display the real [Fig. 3(c)] and imaginary [Fig. 3(d)] parts of the eigenvalues $E_{\pm}$ [Eq. (3)] as a function of $J$ using experimentally obtained values of saturation parameter $\kappa$ and ground-state relaxation rate $\gamma_0$ [18,50]. The blue (pink) shaded regions correspond to the $\mathcal{PT}$-symmetry-broken-like ($\mathcal{PT}$-symmetrylike) regions and the boundary represents EP. For typical parameters as used in Figs. 3(c) and 3(d), we obtain $J_{\rm EP}/2\pi = 0.15$ kHz. When $J < J_{\rm EP}$, the two eigenmodes have the same resonance frequencies but different linewidths. On the other hand, at stronger coupling $J > J_{\rm EP}$, the resonant frequencies of two eigenmodes move in the opposite direction, but their linewidths coincide. We can see that the experiment results are in good agreement with the theoretical prediction.

The observed EPs in atomic ensembles hold great potential for designing EP-enhanced magnetic field sensors, as the coupling strength $J$ is directly related to the

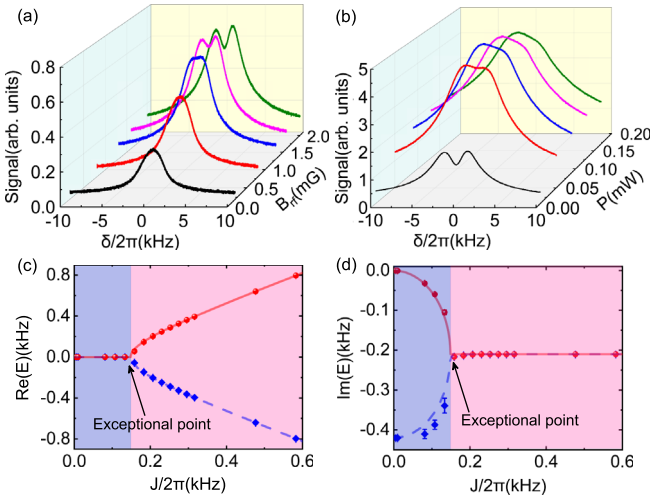


FIG. 3. Experimental results of EPs. (a),(b) Experimental results of OPR signal versus detuning for (a) different rf magnetic fields $B_{\mathrm{rf}}$ from 0.1 to 2 mG and for (b) different probe laser power $P$ from 0.005 to 0.20 mW. (c),(d) Experimentally obtained (c) real and (d) imaginary parts of the system eigenvalues as a function of rf Rabi frequency $J/2\pi$. The red dots and blue squares are obtained from curve fitting the measured OPR spectra to the theoretical result. The error bars are standard deviations obtained from five measurements. The red and blue curves are obtained from the theoretical model using the experimental parameters, and we have used $\gamma_0/2\pi = 0.7$ kHz, $\kappa = 0.3$. The response curve in (a) is the spectrum corresponding to five typical points in (c),(d). Complete experimental data can be found in the Supplemental Material [50].

magnetic field strength. At the second-order EPs, the square-root singularity promises greater signal enhancement for a small perturbation. However, signal enhancement does not always mean increased sensitivity, and some arguments suggest that the sensitivity of the EP sensors are degraded by noise [56–60]. The effect of noise on the signal is that the resonance linewidth (imaginary part of the eigenvalues) increases so that the peak separation is hardly detected in the experiment even if the resonance frequency (real part of the eigenvalues) is split. Therefore, eigenfrequency splitting and measured peak splitting are different. In conventional measurement schemes, the transmission spectra are used to determine the peak splitting [15,16], which rely on the transmission peak degeneracies observed in the transmission spectrum to enhance the signal-to-noise ratio [23,61].

In our scheme, as analyzed in Eq. (4), we use the absorption and dispersion profiles of the OPR signal and make use of the OPR peak degeneracies (OPR-PDs) for observing the peak splitting [50]. As both absorption and dispersion properties are considered, the OPR-PD here is of great advantage for improving the measurement sensitivity. On one hand, as shown in Fig. 4(a), compared with the peak splitting parameter of the absorption signal as $J_{\mathrm{abs}}/2\pi = 0.22$ kHz (pink curve), we find that the peak splitting parameter of OPR signal $J_{\mathrm{OPR}}/2\pi = 0.17$ kHz (blue curve) is much closer to the EP parameter with $J_{\mathrm{EP}}/2\pi = 0.15$ kHz, which means that we obtain a larger signal for the same perturbation. Especially, when $J_{\mathrm{OPR}} < J < J_{\mathrm{abs}}$, it clearly shows that the optical polarization rotation signal is

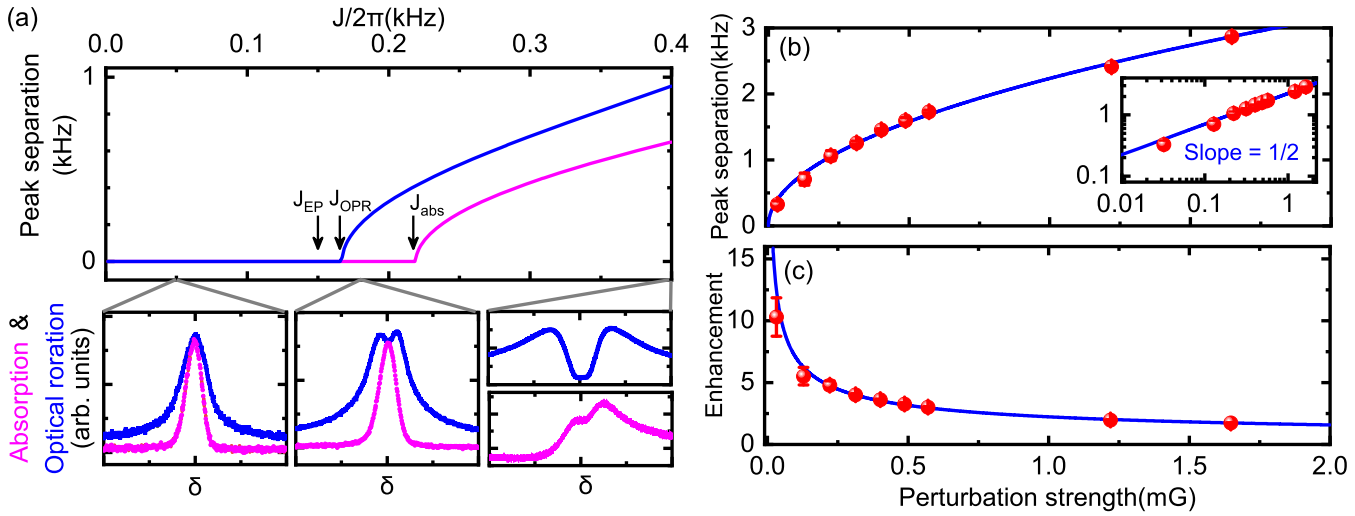


FIG. 4. EP-enhanced sensing with OPR measurement. (a) The peak separation of the OPR signal (blue curve) and absorption spectra (pink curve) as a function of the coupling strength $J/2\pi$. Bottom: snapshots showing the observed optical polarization rotation and absorption spectra versus the detuning $\delta/2\pi$ for three typical coupling strengths, where $J/2\pi = 0.05$, 0.18, 0.4 kHz from left to right. (b) The observed peak separation of OPR magnitude as a function of the perturbation strength. The inset demonstrates a slope of $1/2$ on a logarithmic scale, confirming the existence of exceptional points. (c) Measured enhancement as a function of the perturbation. The sensitivity demonstrates an order enhancement in the proximity of the EP as opposed to a system configuration away from the EP. (b), (c) The red dots indicate experimental data and the error bars are standard deviations obtained from five measurements; the solid blue curves are theoretical results.

split obviously, while the absorption signal does not [middle inset of Fig. 4(a)]. On the other hand, since $J_{\mathrm{OPR}}$ is slightly larger than $J_{\mathrm{EP}}$, it also avoids the collapse of eigenbasis at EPs and thus avoids the excess fundamental noise [62,63].

Figure 4(b) clearly demonstrates a square-root peak splitting in response to changes in the perturbation magnetic field near $J = J_{\mathrm{OPR}}$. As depicted in the inset of Fig. 4(b), the slope of $1/2$ in the corresponding logarithmic plot affirms this behavior. Thanks to the square-root scaling, enhancement of measurement sensitivity can be realized compared with the conventional linear scaling. In our experiments, we have observed an order enhancement in the proximity of the EP compared with the linear scaling away from EP, which corresponds to the case when $J \gg J_{\mathrm{OPR}}$, and is the same as the Hermitian case. The experiment results are in accordance with the theoretical expectations.

It should be stressed that in our system the parameter $\kappa = \Omega^2/(\Gamma\gamma_0)$ can be tuned by adjusting the laser power. Therefore, the corresponding working point $J_{\mathrm{OPR}}$ is real-time controllable, which largely expands the measurement range and opens up realistic opportunities for practical applications in absolute magnetic field measurement in geomagnetism conditions.

In summary, we propose a method for studying non-Hermitian physics in thermal atomic ensembles by making use of the rich energy level structure and couplings. We experimentally observe EPs and realize enhanced sensing of the magnetic field for 1 order of magnitude near the EP. We also propose to measure the optical rotation signal spectrum instead of the transmission spectrum and demonstrate that the peak splitting has a square-root dependence on the perturbation strength, with enhanced sensitivity for detecting the magnetic field. In addition, the position of the EPs can be tuned by adjusting the laser-driven coupling strength, which expands the measurement range. Our scheme can also be generalized to realize high-order EPs by introducing more laser-driven couplings. With the development of advanced nanofabrication technologies, using hollow-core photonic crystal fibers [64,65] or atomic cladding waveguides on a chip [66,67], our scheme is also promising for miniaturization and integration. Our Letter not only provides a new controllable platform for studying EPs and non-Hermitian physics, but also opens up an avenue to design high-sensitivity magnetometers as well as improve the existing measurement methods [47,48].

This work is supported by the Key-Area Research and Development Program of Guangdong Province (Grant No. 2019B030330001), the National Natural Science Foundation of China (NSFC) (Grants No. 12275145, No. 92050110, No. 91736106, No. 11674390, and No. 91836302), and the National Key R&D Program of China (Grant No. 2018YFA0306504).

*ycliu@tsinghua.edu.cn

[1] E. J. Bergholtz, J. C. Budich, and F. K. Kunst, Rev. Mod. Phys. **93**, 015005 (2021).
[2] Y. Ashida, Z. Gong, and M. Ueda, Adv. Phys. **69**, 249 (2020).
[3] L. Feng, R. El-Ganainy, and L. Ge, Nat. Photonics **11**, 752 (2017).
[4] R. El-Ganainy, K. G. Makris, M. Khajavikhan, Z. H. Musslimani, S. Rotter, and D. N. Christodoulides, Nat. Phys. **14**, 11 (2018).
[5] M. A. Miri and A. Alù, Science **363**, eaar7709 (2019).
[6] F. Vollmer and S. Arnold, Nat. Methods **5**, 591 (2008).
[7] J. Zhu, S. K. Ozdemir, Y.-F. Xiao, L. Li, L. He, D.-R. Chen, and L. Yang, Nat. Photonics **4**, 46 (2010).
[8] P. Zijlstra, P. M. R. Paulo, and M. Orrit, Nat. Nanotechnol. **7**, 379 (2012).
[9] Y. Zhi, X.-C. Yu, Q. Gong, L. Yang, and Y.-F. Xiao, Adv. Mater. **29**, 1604920 (2017).
[10] J. Wiersig, Phys. Rev. Lett. **112**, 203901 (2014).
[11] Y.-H. Lai, Y.-K. Lu, M.-G. Suh, Z. Yuan, and K. Vahala, Nature (London) **576**, 65 (2019).
[12] C. Wang, X. Jiang, G. Zhao, M. Zhang, C. W. Hsu, B. Peng, A. D. Stone, L. Jiang, and L. Yang, Nat. Phys. **16**, 334 (2020).
[13] J. Zhang, B. Peng, Ş. K. Özdemir, K. Pichler, D. O. Krimer, G. Zhao, F. Nori, Y.-x. Liu, S. Rotter, and L. Yang, Nat. Photonics **12**, 479 (2018).
[14] S.-B. Lee, J. Yang, S. Moon, S.-Y. Lee, J.-B. Shim, S. W. Kim, J.-H. Lee, and K. An, Phys. Rev. Lett. **103**, 134101 (2009).
[15] W. Chen, Ş. Kaya Özdemir, G. Zhao, J. Wiersig, and L. Yang, Nature (London) **548**, 192 (2017).
[16] H. Hodaei, A. U. Hassan, S. Wittek, H. Garcia-Gracia, R. El-Ganainy, D. N. Christodoulides, and M. Khajavikhan, Nature (London) **548**, 187 (2017).
[17] C. Wang, W. R. Sweeney, A. D. Stone, and L. Yang, Science **373**, 1261 (2021).
[18] B. Peng, S. K. Özdemir, F. Lei, F. Monifi, M. Gianfreda, G. L. Long, S. Fan, F. Nori, C. M. Bender, and L. Yang, Nat. Phys. **10**, 394 (2014).
[19] L. Chang, X. Jiang, S. Hua, C. Yang, J. Wen, L. Jiang, G. Li, G. Wang, and M. Xiao, Nat. Photonics **8**, 524 (2014).
[20] B. Zhen, C. W. Hsu, Y. Igarashi, L. Lu, I. Kaminer, A. Pick, S.-L. Chua, J. D. Joannopoulos, and M. Soljačić, Nature (London) **525**, 354 (2015).
[21] J.-h. Park, A. Ndao, W. Cai, L. Hsu, A. Kodigala, T. Lepetit, Y.-h. Lo, and B. Kanté, Nat. Phys. **16**, 462 (2020).
[22] K. Ding, G. Ma, M. Xiao, Z. Q. Zhang, and C. T. Chan, Phys. Rev. X **6**, 021007 (2016).
[23] R. Kononchuk, J. Cai, F. Ellis, R. Thevamaran, and T. Kottos, Nature (London) **607**, 697 (2022).
[24] X. Yang, J. Li, Y. Ding, M. Xu, X.-F. Zhu, and J. Zhu, Phys. Rev. Lett. **128**, 065701 (2022).
[25] Z. Xiao, H. Li, T. Kottos, and A. Alù, Phys. Rev. Lett. **123**, 213901 (2019).
[26] Y. Sun, W. Tan, H.-q. Li, J. Li, and H. Chen, Phys. Rev. Lett. **112**, 143903 (2014).
[27] S. Assawaworrarit, X. Yu, and S. Fan, Nature (London) **546**, 387 (2017).

[28] P.-Y. Chen, M. Sakhdari, M. Hajizadegan, Q. Cui, M. M.-C. Cheng, R. El-Ganainy, and A. Alù, Nat. Electron. **1**, 297 (2018).
[29] H. Jing, S. K. Özdemir, X.-Y. Lü, J. Zhang, L. Yang, and F. Nori, Phys. Rev. Lett. **113**, 053604 (2014).
[30] H. Xu, D. Mason, L. Jiang, and J. G. Harris, Nature (London) **537**, 80 (2016).
[31] M. Naghiloo, M. Abbasi, Y. N. Joglekar, and K. W. Murch, Nat. Phys. **15**, 1232 (2019).
[32] W. Chen, M. Abbasi, B. Ha, S. Erdamar, Y. N. Joglekar, and K. W. Murch, Phys. Rev. Lett. **128**, 110402 (2022).
[33] M. Abbasi, W. Chen, M. Naghiloo, Y. N. Joglekar, and K. W. Murch, Phys. Rev. Lett. **128**, 160401 (2022).
[34] J. Li, A. K. Harter, J. Liu, L. de Melo, Y. N. Joglekar, and L. Luo, Nat. Commun. **10**, 855 (2019).
[35] L. Ding, K. Shi, Q. Zhang, D. Shen, X. Zhang, and W. Zhang, Phys. Rev. Lett. **126**, 083604 (2021).
[36] P. Peng, W. Cao, C. Shen, W. Qu, J. Wen, L. Jiang, and Y. Xiao, Nat. Phys. **12**, 1139 (2016).
[37] R. Lefebvre, O. Atabek, M. Šindelka, and N. Moiseyev, Phys. Rev. Lett. **103**, 123003 (2009).
[38] H. Cartarius, J. Main, and G. Wunner, Phys. Rev. Lett. **99**, 173003 (2007).
[39] A. I. Magunov, I. Rotter, and S. I. Strakhova, J. Phys. B **32**, 1489 (1999).
[40] O. Latinne, N. J. Kylstra, M. Dörr, J. Purvis, M. Terao-Dunseath, C. J. Joachain, P. G. Burke, and C. J. Noble, Phys. Rev. Lett. **74**, 46 (1995).
[41] M. V. Berry and D. H. J. O'Dell, J. Phys. A **31**, 2093 (1998).
[42] Y. Wu, W. Liu, J. Geng, X. Song, X. Ye, C.-K. Duan, X. Rong, and J. Du, Science **364**, 878 (2019).
[43] I. K. Kominis, T. W. Kornack, J. C. Allred, and M. V. Romalis, Nature (London) **422**, 596 (2003).
[44] D. Budker and M. Romalis, Nat. Phys. **3**, 227 (2007).
[45] H. Bao, J. Duan, S. Jin, X. Lu, P. Li, W. Qu, M. Wang, I. Novikova, E. E. Mikhailov, K.-F. Zhao, K. Mølmer, H. Shen, and Y. Xiao, Nature (London) **581**, 159 (2020).
[46] Y. Wu, J. Guo, X. Feng, L. Chen, C.-H. Yuan, and W. Zhang, Phys. Rev. Appl. **14**, 064023 (2020).
[47] M. Jing, Y. Hu, J. Ma, H. Zhang, L. Zhang, L. Xiao, and S. Jia, Nat. Phys. **16**, 911 (2020).
[48] J. A. Sedlacek, A. Schwettmann, H. Kübler, R. Löw, T. Pfau, and J. P. Shaffer, Nat. Phys. **8**, 819 (2012).
[49] L. S. Cutler, Metrologia **42**, S90 (2005).
[50] See Supplemental Material at http://link.aps.org/supplemental/10.1103/PhysRevLett.130.263601 for the derivation of the effective Hamiltonian and the OPR signal, extracting eigenfrequencies, and more experiment results.
[51] X.-L. Zhang, T. Jiang, and C. T. Chan, Light Sci. Appl. **8**, 88 (2019).
[52] F. Yang, Y.-C. Liu, and L. You, Phys. Rev. A **96**, 053845 (2017).
[53] Z. Feng and X. Sun, Phys. Rev. Lett. **129**, 273601 (2022).
[54] I. Mandal and E. J. Bergholtz, Phys. Rev. Lett. **127**, 186601 (2021).
[55] S. Jeon, G. Jang, H. Choi, and S. Park, IEEE Trans. Magn. **46**, 1943 (2010).
[56] N. A. Mortensen, P. A. D. Gonçalves, M. Khajavikhan, D. N. Christodoulides, C. Tserkezis, and C. Wolff, Optica **5**, 1342 (2018).
[57] W. Langbein, Phys. Rev. A **98**, 023805 (2018).
[58] M. Zhang, W. Sweeney, C. W. Hsu, L. Yang, A. D. Stone, and L. Jiang, Phys. Rev. Lett. **123**, 180501 (2019).
[59] C. Chen, L. Jin, and R.-b. Liu, New J. Phys. **21**, 083002 (2019).
[60] H.-K. Lau and A. A. Clerk, Nat. Commun. **9**, 4320 (2018).
[61] Q. Geng and K.-D. Zhu, Photonics Res. **9**, 1645 (2021).
[62] J. Wiersig, Nat. Commun. **11**, 2454 (2020).
[63] H. Wang, Y.-H. Lai, Z. Yuan, M.-G. Suh, and K. Vahala, Nat. Commun. **11**, 1610 (2020).
[64] P. Londero, V. Venkataraman, A. R. Bhagwat, A. D. Slepkov, and A. L. Gaeta, Phys. Rev. Lett. **103**, 043602 (2009).
[65] M. R. Sprague, P. S. Michelberger, T. F. M. Champion, D. G. England, J. Nunn, X.-M. Jin, W. S. Kolthammer, A. Abdolvand, P. S. J. Russell, and I. A. Walmsley, Nat. Photonics **8**, 287 (2014).
[66] L. Stern, B. Desiatov, N. Mazurski, and U. Levy, Nat. Commun. **8**, 14461 (2017).
[67] R. Ritter, N. Gruhler, H. Dobbertin, H. Kübler, S. Scheel, W. Pernice, T. Pfau, and R. Löw, Phys. Rev. X **8**, 021032 (2018).